Transient shear banding during startup flow: Insights from nonlinear simulations

Shweta Sharma (श्वेता शर्मा),[1] Yogesh M. Joshi (योगेश मो. जोशी),[1, a)] and V. Shankar (वि. शंकर)[1, b)]

Department of Chemical Engineering, Indian Institute of Technology Kanpur, Kanpur 208016, India

We study the dynamics of shear startup of Johnson-Segalman and non-stretching Rolie-Poly models using nonlinear simulations. We consider startup to shear rates in both monotonic and nonmonotonic regions of the constitutive curve. For the Johnson-Segalman model, which exhibits a shear stress overshoot during startup, our nonlinear simulations show that transient shear banding is absent regardless of whether the start-up shear rate is in the monotonic or nonmonotonic regions of the constitutive curve. In the latter case, while there is clearly an inhomogeneity *en route* to the banded state, the magnitude of the extent of banding is not substantially large compared to that of the eventual banded state. Marked inhomogeneity in the velocity profile is predicted for the non-stretching Rolie-Poly model only if the solvent to solution viscosity ratio is smaller than $O(10^{-3})$, but its occurrence does not appear to have any correlation with the stress overshoot during startup. The comparison of the present nonlinear results with the results obtained within the framework of linearized dynamics show that nonlinearities have a stabilizing effect and mitigate the divergence of perturbations (as predicted within the linearized dynamics) during shear startup. We argue that the neglect of inertia in the nonlinear simulations is not self-consistent if the solvent to solution viscosity ratio is very small, and that inertial effects need to be included in order to obtain physically realistic results. Furthermore, our study demonstrates a pronounced sensitivity of shear startup in the nonstretching Rolie Poly model when a random white noise with zero mean is used as the initial perturbation. Finally, this study clearly emphasizes that stress overshoot during shear startup does not always result in transient shear banding, notwithstanding whether the shear rates is in the monotonic or nonmonotonic part of the constitutive curve.

[a)] Electronic mail: joshi@iitk.ac.in

[b)] Electronic mail: vshankar@iitk.ac.in

I. INTRODUCTION

The flow characteristics and rheology of viscoelastic fluids are often determined by subjecting them to shear and extensional flows. Several constitutive models have been proposed in the literature to predict the experimental results [1–19]. When viscoelastic fluids undergo shear and extensional flows, they are often susceptible to various instabilities [1–9]. Shear banding is one such example of an instability exhibited by viscoelastic materials with a non-monotonic constitutive relation between shear stress and shear rate. When such a material is subjected to a planar Couette flow, with the applied shear rate in the nonmonotonic region of the constitutive curve, the linear velocity profile becomes unstable and transforms into bands of two distinct shear rates. The shear rates of the two bands lie on the stable branches of the constitutive curve.

Shear banding that ensues after the flow has reached a steady state is referred to as steady-state shear banding. Transient banding, in contrast, occurs when the flow is evolving towards the banded or homogeneous steady state, with the presence of two or more bands with distinctly different shear rates characterized by a sharp transition zone between the bands. When the eventual steady state is banded, it is unambiguous to identify transient shear banding only if the velocity profiles during evolution exhibit substantially pronounced banding compared to the eventual steady-state banding [20].

In recent studies, transient shear banding is often quantified by monitoring the difference between maximum and minimum shear rates, which has been dubbed as the 'degree of banding' [20 and 21]. If the steady state is homogeneous, then the evolution of degree of banding with time can transiently increase to attain a maximum and then decrease to zero. If the steady state is banded, then the presence of transient shear banding can be ascertained only if degree of banding shows a transient peak of substantially higher magnitude compared to its eventual steady-state value. The evolution of second derivative of velocity in the direction of momentum diffusion has also been suggested in literature to determine the presence of transient shear banding [22–24]. The thickness of the interface between two bands must be much smaller than the width of the bands, in order for the two bands to be distinguishable; hence, transient flow inhomogeneities during shear startup may not always be designated as transient shear banding. Cheng et al. [24] conducted experiments using a shear thinning wormlike micellar solution in the Taylor-Couette geometry of a rheometer,

where they observed banding-like inhomogeneities. To distinguish between shear banding and transient inhomogeneities, they examined the third derivative of velocity with respect to the wall normal direction. The presence of cusplike peaks in the third derivative indicates the presence of shear banding. Therefore, in such cases, the second or third derivative of velocity provides a more reliable means of identifying shear banding. However, during the course of our study, we found that this method of distinguishing between inhomogeneities and banding is more suitable when well-defined regions of distinct shear rates exist. Moreover, to facilitate comparison of our results with those presented in the literature, we have adopted the degree of banding metric in this study.

The stability of the homogeneous steady state of a shear flow was first studied by Yerushalmi et al. [25] who proposed a model-independent or fluid-universal criterion for existence of steady state shear banding in shear startup flow. The authors stated that "It is shown that all values of the steady shear rate where the flow curve exhibits a zero or negative slope the flow is unstable." This criterion has been validated using various constitutive models with a nonmonotonic region where shear stress decreases as a function of shear rate [26–42].

A fluid-universal or model-independent criterion for existence of transient shear banding during shear startup flow has been proposed by Moorcroft and Fielding [20 and 43]. According to this criterion, in a shear startup flow, if shear stress shows an overshoot, then during the time duration in which shear stress shows a negative slope as a function of time or strain, the shear startup flow should become unstable and form bands of different shear rates transiently. The authors carried out a modal stability analysis by freezing the base state at a given instant, treating the flow to be quasi-steady (this procedure is referred to as the 'frozen-time' analysis) to derive the criterion for transient banding. In our previous study [44], we discussed in detail the restrictive nature of the criterion based on the assumptions utilised to obtain the simplified criterion. In brief, these assumptions are (i) shear startup must be in the high shear-rate region, (ii) frozen time analysis can be used as a tool to obtain the signature of transient shear banding, (iii) absence of Hopf bifurcation, and (iv) only one real part of transient eigenvalue is positive at any time.

Moorcroft and Fielding [20] examined the shear startup of stretching and non-stretching Rolie-Poly and Giesekus models using the frozen time analysis, linearized evolution of perturbations, and nonlinear simulations to check the validity of the criterion. They found

that the results obtained using the non-stretching Rolie-Poly model validated the criterion, however, for the stretching Rolie-Poly and Giesekus models, transient shear banding was not observed even in presence of stress overshoot. The authors argued that since transient shear banding is an elastic instability, the models that show stress overshoot at same magnitude of strain qualify to show transient shear banding. Fielding [45] subsequently noted that while the criterion is useful, it may not be universal.

The transient shear banding criterion for shear startup flow has been tested experimentally and numerically and it has been found to be consistent in some cases, but is not universally applicable [33, 34, 44, 46–63] as discussed in Section II of our previous study [44]. Transient and steady state shear banding has been observed in shear startup of entangled polymer solutions which can be influenced by flow-concentration coupling [36, 37, 51, 64–67]. Transient shear banding in shear startup flow of wormlike micellar systems has also been explored, when the startup shear rate is such that the steady state is also banded or using geometries that exhibit high shear stress inhomogeneity [34, 35, 56, 60, 68–70]. Hu et al. [60] observed transient shear banding during shear startup of wormlike micellar solutions using cone and plate geometry. In this study, we focus on shear startup of viscoelastic constitutive models that can predict both monotonic and nonmonotonic constitutive curves and have no coupling with concentration (Rolie-Poly model) [29, 31, 32, and 48] and can fit experimental results of wormlike micellar solutions (Johnson-Segalman model [27]).

In our earlier study [44], we had analyzed the transient shear banding criterion for shear startup flow using Johnson-Segalman, non-stretching Rolie-Poly, and Giesekus models within the framework of the frozen-time analysis and the fundamental matrix method. The frozen-time approach is valid only if the transient growth rate is significantly higher than the rate of change of base-state evolution. In the fundamental matrix method [71–74], the evolution of linearized perturbations can be obtained along with the evolution of base state. This method also provides the growth rate of perturbations maximised over all possible initial conditions and consequently yields more robust results compared to frozen time analysis. We showed that the assumptions made to derive the criterion for transient shear banding [20] are restrictive and that there is no consistent link between positive transient eigenvalue and stress overshoot. We also showed that the transiently positive eigenvalue does not lead to growth of linearized perturbations for the Johnson-Segalman model. Conversely, using the Giesekus model, we showed that even a transiently positive eigenvalue is not necessary

for transient growth of linearized perturbations.

For some cases of shear startup of non-stretching Rolie-Poly model, we found agreement between stress overshoot, transiently positive eigenvalue and growth of perturbations (see Figs. 6-7 of Ref. [44]), as reported earlier by Moorcroft and Fielding [20]. We attributed the contrasting results obtained using the Johnson-Segalman and non-stretching Rolie-Poly models to the difference in orders of magnitude of ratio of solvent to solution viscosity: $\eta_s = 0.115$ for the Johnson-Segalman model and 10^{-5} for non-stretching Rolie-Poly models. For the non-stretching Rolie-Poly model, at high shear rates, we showed that the maximum transient eigenvalue diverges on decreasing the ratio of solvent to solution viscosity. We also argued that if transient growth rate becomes significantly high, then inertial effects can no longer be ignored. We found that the growth of linearized perturbations reduced significantly in the presence of inertia suggesting that there may not be any transient shear banding if shear startup flow is carried out for higher ratios of solvent to solution viscosity. If the ratio of solvent to solution viscosity is less than $O(10^{-3})$, then inclusion of inertia may regularise the eigenvalue and perturbations. However, this conclusion was based on an approximate solution in which inertia is considered only during evolution of perturbations and not during base state. Furthermore, the growth of linearized perturbations also does not necessarily guarantee the presence of transient shear banding since the nonlinear terms are ignored. Therefore, it is of interest to examine whether transient shear banding prevails in the scenario where the nonlinear terms are also considered.

In this work, we study the shear startup flow of the Johnson-Segalman and non-stretching Rolie-Poly models using full nonlinear simulations by imposing perturbations at the beginning of the shear startup. It is important to highlight that, as we revisit the criterion of transient shear banding for shear startup flow (Ref. [20]), we specifically employ the non-stretching Rolie-Poly model. As stated in Ref. [20], stretching Rolie Poly model lacks the capability to show elastic instability, we restrict the study of transient dynamics only to the non-stretching Rolie Poly model. The study focuses on shear startup under the same parameters values discussed in Ref. [20] to facilitate a comparative analysis of results. We discuss both the models and governing equations, and highlight the issue of realistic initial amplitude of perturbations to study transient shear banding in Sec. II. We then explore the effect of initial amplitude of perturbation on transient dynamics of shear startup flow in presence and absence of inertia in Sec. III A. We also study the effect of decreasing ratio of

solvent to solution viscosity and effect of inertia on transient dynamics of shear startup flow and examine whether inertia (non-zero Re) regularises the effect of low ratio of solvent to solution viscosity in Sec. III B. We discuss the salient conclusions of this study in Sec. IV.

II. MODELS AND GOVERNING EQUATIONS

We use the Johnson-Segalman and non-stretching Rolie-Poly models to analyse shear startup of viscoelastic fluids. We consider an incompressible viscoelastic fluid between two parallel plates that are infinite in the x^* and z^* directions and confined in the y-direction, with a gap H between the plates. Both plates are at rest for time $t^* < 0$, but for time $t^* \geq 0$, the top plate moves at a steady velocity U in the x^* direction. The variables in this manuscript that include a superscript $*$ are dimensional, while those without a superscript are dimensionless. In this case, the Cauchy momentum equation is as follows:

$$-\nabla p^* + \nabla \cdot \underset{\approx}{\Sigma}^* + \underset{\sim}{f}^* = \rho \left(\frac{\partial \underset{\sim}{u}^*}{\partial t^*} + \underset{\sim}{u}^* \cdot \nabla \underset{\sim}{u}^* \right), \tag{1}$$

The above equation simplified for unidirectional simple shear flow as:

$$-\nabla p^* + \nabla \cdot \underset{\approx}{\Sigma}^* + \underset{\sim}{f}^* = \rho \frac{\partial \underset{\sim}{u}^*}{\partial t^*}, \tag{2}$$

In Eqs. 1-2, p^* represents the pressure, $\underset{\sim}{f}^*$ denotes the body forces ρ is the density of the fluid, $\underset{\sim}{u}^*$ is the velocity field, and $\underset{\approx}{\Sigma}^*$ is the total stress tensor. To simplify the analysis, we assume that the body forces can be neglected, no pressure gradient is applied, and the flow is unidirectional and incompressible. In this work, we seek unidirectional and fully-developed solutions, so the pressure gradient in the x and z direction will remain zero even during shear-startup, since the continuity equation is exactly satisfied by this flow field ($\nabla \cdot \underset{\sim}{u}^* = 0$). However, in the y-direction, a pressure gradient develops in order to balance the gradient of the yy component of stress in the y-direction. This is akin to the hydrostatic distribution of pressure in the vertical direction of in a horizontally oriented channel, with the flow occurring in the horizontal direction. In the absence of an externally applied pressure difference, a nontrivial pressure gradient in the flow direction will be generated in an incompressible flow only when the continuity equation is not trivially satisfied, and the flow field becomes two-dimensional with (at least) two nonzero velocity components. One

noteworthy example is lubricating flow in a slider block [75], where the slowly varying cross-section results in the generation of a pressure gradient to ensure mass conservation. For this reason, in the ensuing analysis, we ignore the pressure term in the x-momentum equation; this framework has been used in almost all of the literature on steady-state/transient shear banding [20, 21, 45, 76, and 77].

We consider the total stress to be equal to the sum of viscoelastic stress and Newtonian solvent stress contributions:

$$\underset{\approx}{\Sigma}^* = \underset{\approx}{\sigma}^* + 2\bar{\eta}_s \underset{\approx}{\dot{\gamma}}^*, \tag{3}$$

where, $\underset{\approx}{\sigma}^*$ is the viscoelastic stress, $\bar{\eta}_s$ is the viscosity of solvent in a polymeric or wormlike micellar solution, and $\underset{\approx}{\dot{\gamma}}^* = \frac{1}{2}(\nabla \underset{\sim}{u}^* + (\nabla \underset{\sim}{u}^*)^T)$ is the shear rate tensor. We use the Johnson-Segalman [27] and the Rolie-Poly [32] models for the viscoleastic stress ($\underset{\approx}{\sigma}^*$). Both models are augmented by an additional stress diffusion term for unique stress selection in the non-monotonic region of the flow curve in our nonlinear simulations [20, 40, and 78]. The models are made dimensionless as follows: $\underset{\approx}{\sigma} = \dfrac{\underset{\approx}{\sigma}^*}{((\bar{\eta}_s + \bar{\eta}_p)/\tau)}$, $t = t^*/\tau$, $\underset{\sim}{u} = \underset{\sim}{u}^*/U$. In the above expressions, $\bar{\eta}_p$ is the contribution of polymer to the zero shear viscosity of the solution and τ is the relaxation time of the fluid. In the case of Rolie-Poly model, $\tau = \tau_D$, which represents the reptation time, and for Johnson-Segalman model $\tau = \lambda$ which is the longest relaxation time. The relevant dimensionless groups are the Weissenberg number, $Wi = \dfrac{\tau U}{H}$ which represents non-dimensional shear rate, Reynolds number $Re = \dfrac{\rho U H}{\bar{\eta}_s + \bar{\eta}_p}$, and the ratio of solvent viscosity to the zero shear viscosity of the solution, $\eta_s = \dfrac{\bar{\eta}_s}{\bar{\eta}_s + \bar{\eta}_p}$. We also assume no-slip boundary conditions i.e., $u(y=1) = U$ and $u(y=0) = 0$. The dimensionless form of Cauchy momentum equation is given below:

$$Re\frac{\partial u}{\partial t} = \frac{\partial \sigma_{xy}}{\partial y} + \eta_s Wi \frac{\partial^2 u}{\partial y^2} \tag{4}$$

Johnson-Segalman model - The Johnson-Segalman (hereafter JS) model [27] was developed to introduce non-affine motion in the upper-convected Maxwell (UCM) model by replacing the upper-convected derivative with the Gordon-Schowalter derivative [27, 79, and 80]. The degree of non-affine motion is governed by the slip parameter ξ. If $\xi = 0$, the JS constitutive equations yields the UCM model and if $\xi = 2$, it reduces to the Lower Convective Maxwell (LCM) model [79]. The constitutive equation of the JS model is given by the

following equation

$$\underset{\approx}{\sigma}^{*} + \lambda \overset{\square}{\underset{\approx}{\sigma}}^{*} = 2\bar{\eta}_p \underset{\approx}{\dot{\gamma}}^{*} \tag{5}$$

and the Gordon-Schowalter derivative $\overset{\square}{\underset{\approx}{\sigma}}$ [79] is

$$\overset{\square}{\underset{\approx}{\sigma}}^{*} = \left(1 - \frac{\xi}{2}\right) \overset{\triangledown}{\underset{\approx}{\sigma}}^{*} + \left(\frac{\xi}{2}\right) \overset{\triangle}{\underset{\approx}{\sigma}}^{*} \tag{6}$$

where λ is the longest relaxation time of the polymeric solution, $\bar{\eta}_p$ is the contribution of polymer to the zero shear viscosity of the solution and ξ is fixed as 0.01 for the results shown in this manuscript. (We have verified that the results are largely insensitive to the specific value of ξ chosen.) The upper-convected and the lower-convected derivatives are $\overset{\triangledown}{\underset{\approx}{\sigma}} = \frac{D\boldsymbol{\sigma}}{Dt} - (\nabla \boldsymbol{u})^T \cdot \boldsymbol{\sigma} - \boldsymbol{\sigma} \cdot (\nabla \boldsymbol{u})$ and $\overset{\triangle}{\underset{\approx}{\sigma}} = \frac{D\boldsymbol{\sigma}}{Dt} + (\nabla \boldsymbol{u}) \cdot \boldsymbol{\sigma} + \boldsymbol{\sigma} \cdot (\nabla \boldsymbol{u})^T$, respectively, where, $\frac{D}{Dt}$ is the substantial derivative [81]. The diffusion term is augmented to the JS model constitutive equation for the unique stress selection [40]. The simplified dimensionless component-wise equations of the model for unidirectional simple shear flow are

$$\frac{\partial \sigma_{xy}}{\partial t} = \left(-\left(\frac{\xi}{2}\right)\sigma_{xx} + \left(1 - \frac{\xi}{2}\right)\sigma_{yy} + (1 - \eta_s)\right)\dot{\gamma} Wi - \sigma_{xy} + D\frac{\partial^2 \sigma_{xy}}{\partial y^2}, \tag{7}$$

$$\frac{\partial \sigma_{xx}}{\partial t} = 2\left(\left(1 - \frac{\xi}{2}\right)\sigma_{xy}\right)\dot{\gamma} Wi - \sigma_{xx} + D\frac{\partial^2 \sigma_{xx}}{\partial y^2}, \tag{8}$$

$$\frac{\partial \sigma_{yy}}{\partial t} = -\left(\xi \sigma_{xy}\right)\dot{\gamma} Wi - \sigma_{yy} + D\frac{\partial^2 \sigma_{yy}}{\partial y^2}. \tag{9}$$

Here, $\boldsymbol{D}$ is the dimensionless stress diffusion coefficient and the dimensional stress diffusion coefficient is $\boldsymbol{D}^* = \frac{DH^2}{\lambda}$.

Rolie-Poly model - The Rolie-Poly model is a single-mode molecular model for entangled polymer melts with its name derived from ROuse LInear Entangled POLYmers model. This model was developed by Likhtman and Graham by simplification of the Doi-Edwards tube model [28 and 32]. This model also accounts for most of the molecular processes, including reptation, convective constraint release (CCR), chain stretch, retraction, and contour length fluctuations. The constitutive equation of the model can be expressed as follows

$$\left(\underset{\approx}{\sigma}^{*} - \underset{\approx}{I}\right) + \tau_D \overset{\triangledown}{\underset{\approx}{\sigma}}^{*} = -2\frac{\tau_D}{\tau_R}\left(1 - \sqrt{\frac{3}{\mathrm{tr}\left(\underset{\approx}{\sigma}^{*}\right)}}\right)\left(\underset{\approx}{\sigma}^{*} + \beta\left(\underset{\approx}{\sigma}^{*} - \underset{\approx}{I}\right)\left(\sqrt{\frac{3}{tr\left(\underset{\approx}{\sigma}^{*}\right)}}\right)^{-2\delta}\right), \tag{10}$$

where β determines the effectiveness of the convective constraint release mechanism, $\delta = \frac{1}{2}$ following [32 and 82] which fixes the strength of convective constraint release. Here, $\underset{\approx}{I}$ is the identity tensor. Also, τ_D determines the contribution of reptation to relaxation mechanism, τ_R shows the contribution of chain stretching to relaxation mechanism. The number of entanglements is represented by $Z\left(Z = \dfrac{\tau_D}{3\tau_R}\right)$, which consequently fixes the two relaxation times.

Likhtman and Graham [32] further simplified the model by considering $\tau_R \to 0$ and $\mathrm{tr}\left(\underset{\approx}{\sigma}^*\right) = 3 + \Delta$ (here $\Delta = 0$ because $\tau_R \to 0$ and $Z \gg 100$). The simplified model is known as non-stretching Rolie-Poly model, referred hereafter as the nRP model, whose constitutive equation is given by:

$$\left(\underset{\approx}{\sigma}^* - \underset{\approx}{I}\right) + \tau_D \overset{\nabla}{\underset{\approx}{\sigma}}^* = -\frac{2}{3}\tau_D \left(\mathrm{tr}\left(\underset{\sim}{\nabla}^* \underset{\sim}{u}^* \cdot \underset{\approx}{\sigma}^*\right)\right)\left(\underset{\approx}{\sigma}^* + \beta\left(\underset{\approx}{\sigma}^* - \underset{\approx}{I}\right)\right). \tag{11}$$

The component-wise equations of the nRP model augmented with stress diffusion coefficient, D in nondimensional form for unidirectional simple shear flow are as follows:

$$\frac{\partial \sigma_{xy}}{\partial t} = Wi\dot{\gamma}\left(\sigma_{yy} - \frac{2}{3}\sigma_{xy}^2(1+\beta)\right) - \sigma_{xy} + D\frac{\partial^2 \sigma_{xy}}{\partial y^2}, \tag{12}$$

$$\frac{\partial \sigma_{yy}}{\partial t} = \frac{2}{3}Wi\dot{\gamma}\left(\beta\sigma_{xy} - \sigma_{yy}\sigma_{xy}(1+\beta)\right) - (\sigma_{yy} - 1) + D\frac{\partial^2 \sigma_{yy}}{\partial y^2}. \tag{13}$$

Here, D is the dimensionless stress diffusion coefficient and the dimensional stress diffusion coefficient is $D^* = \dfrac{DH^2}{\tau_D}$ [20]. The results for the nRP model are obtained using $\beta = 0.6$ and $\beta = 1$ for start-up to non-monotonic and monotonic regions of the constitutive curve, respectively. We carry out full non-linear simulations for simple shear flow and solve Eqs. 2, Eqs. 7-9 and Eqs. 12-13. In this study, we impose a perturbation as initial condition for $\underset{\sim}{u}$ and $\underset{\approx}{\sigma}$ which is expressed in index notation as follows:

$$u_i = u_i^0 + A\sin(n\pi y), \qquad \sigma_{ij} = \sigma_{ij}^0 + A\cos(n\pi y), \tag{14}$$

where A is the amplitude of the sine or cosine wave, n fixes its wavelength, u_i represents the components of the velocity vector, σ_{ij} represents the components of the stress tensor (the chosen perturbation as initial condition is inspired from Ref. [20] for comparative analysis of results. In Ref. [20], the sinusoidal wave perturbation imposed is also multiplied by a white noise prefactor; however, we study the effect of sinusoidal and white noise initial conditions

separately.) Here, $u_i^0 = y$ and σ_{ij}^0 is a constant, 10^{-5}. (The results obtained are independent of the precise value of σ_{ij}^0, if its magnitude is much smaller than unity. The perturbations to the various components of the stress tensor are chosen as cosines, so that the velocity perturbation can be written in terms of sines, and thus the no-slip boundary condition gets satisfied at $y = 0$ and 1. In this manuscript, n (in Eq. 14) is fixed as 1, as it yields the most unstable mode and A is considered as 10^{-1}, 10^{-4}, and 10^{-7}. In this study, we also use random noise as initial perturbation to velocity field and stress tensor. We use these perturbations according to the equations which are expressed in index notation below:

$$u_i = u_i^0 + A\,R(y), \qquad \sigma_{ij} = \sigma_{ij}^0 + A\,R(y), \tag{15}$$

where $R(y)$ is generated from a set of random numbers distributed uniformly with a mean of 0 and a width of 1 as well as it is same for u_i and σ_{ij}. We have fixed the stress diffusion parameter $D = 10^{-2}$ in this study. Furthermore, we have verified that the results (shown in Fig. 2) obtained from the JS model are not influenced by the slip parameter, ξ, while the results (shown in Fig. 3) from the nRP model are not affected by the parameter β.

In our discussions below, in the interests of clarity, we have incorporated some of the data concerning linearized dynamics from our earlier work (Ref. [44]), duly acknowledged at the relevant locations. For details on the methodology for determining the maximum amplitude of linearized perturbations and transient maximum eigenvalue, readers are referred to Section III of Ref. [44].

A. A note on the magnitude of shear rate initial condition

In the absence of inertia, it is not possible to specify the initial amplitude of the shear rate because the Cauchy momentum equation is devoid of any acceleration in the inertialess limit. In this limit, the initial value of the shear rate is actually dictated by the initial value of σ_{xy} as given by the Cauchy momentum equation (Eq. 4) in the absence of inertia: $\dot{\gamma}(t=0) = \sigma_{xy}(t=0)/(\eta_s Wi)$. As a consequence, for $\eta_s \ll 1$, the initial shear rate perturbation is $O(\eta_s^{-1})\sigma_{xy}(t=0)$, i.e., it is much larger than the magnitude of the (prescribed) stress perturbation. Thus, for $\eta_s \ll 1$, if we impose an $O(1)$ stress perturbation at $t = 0$, the shear rate perturbations become much larger than unity. Note that the step change in the shear rate, in the shear start-up protocol, is only an $O(1)$ quantity. It is therefore unrealistic to

impose a large (i.e. $\gg O(1)$) shear rate perturbation as an initial condition in the nonlinear simulations. The initial conditions in our numerical simulations are intended to mimic inevitable (spontaneous) perturbations that would be present in an experiment. Thus, in order for the initial conditions to be physically realistic, one should not have the shear rate perturbation magnitudes to be much larger than the $O(1)$ base state itself. In order to address this issue, especially in the limit of small η_s, it is necessary to prescribe the initial shear stress perturbation amplitudes in a manner that the initial shear rate perturbation is at most $O(10^{-1})$ (i.e. 10% of the imposed shear rate jump in the startup flow).

It is useful here to clarify what the imposed initial perturbations are purported to mimic in our simulations. We consider spontaneous "external" disturbances that are unavoidable in a laboratory experiment, as is customary in the framework of hydrodynamic stability [83 and 84]. However, there is another formulation, referred to as the fluctuating Navier-Stokes equations [85], wherein thermal fluctuations are included in the Navier-Stokes equations in the context of a Newtonian fluid. In that formulation, valid for a fluid at thermal equilibrium, the magnitude of the stress fluctuations is governed by a fluctuation-dissipation theorem and is proportional to $\sqrt{k_B T \eta / V}$, where η is the fluid viscosity, k_B is the Boltzmann constant, T is the temperature in Kelvin and V is a representative system volume. Here, a reasonable estimate for volume is $V \sim H^3$, where H is the gap width. In the context of stability of cylindrical jets [86], $V \sim d^3$ where d is the jet diameter. Indeed it was shown that only for 'nanojets' with diameter of a few nanometers, thermal stress fluctuations were shown to affect the stability of jets. For the present geometry, if one uses $H = 1$ mm, and $\eta = 1$ Pa s, $T = 300$ K, then one obtains the magnitude of thermal stress flucutations to be around 2×10^{-6} Pa. For the same parameters, the macroscopic shear stress can be estimated as $\mu V / H$. For $V = 1$ mm/s, shear stress is 1 Pa. Even if one assumes the magnitude of non-thermal stress disturbances in experiments to be 0.1% of the macroscopic stress, this yields 10^{-3} Pa, which is three orders of magnitude larger than that of spontaneous thermal fluctuations. Such thermally-induced fluctuations are referred to as "internal" fluctuations by Ref. [87] and Ref. [86]. However, when a system is unstable to infinitesimal disturbances, the physical origin of the perturbations is irrelevant, and the given state is bound to lose its stability.

We also calculate the order of initial shear rate perturbation for both the models. For the JS model, consider the case of $Re = 0$, where the initial shear rate perturbation is

approximately 10^{-1}, 10^{-4}, and 10^{-7} for $Wi = 12$ and $\eta_s = 0.16$. Conversely, for the nRP model in the absence of inertia, providing initial conditions directly to the shear rate is not feasible. Instead, the initial values of the shear rate are determined by the initial stress perturbation $\sigma_{xy}(t = 0)$ through the Cauchy momentum equation (Eq. 4). As $\dot{\gamma}(t = 0) = \sigma_{xy}(t = 0)/Wi\eta_s$, the shear rate perturbations become significantly larger than the stress perturbations. For $A = 10^{-1}$, the initial shear rate perturbation is on the order of 10^2 (equivalent to 10^4% of the base state shear rate for $\eta_s = 10^{-4}$ and $Wi = 30$). Similarly, with $A = 10^{-4}$, the initial shear rate perturbation is on the order of 10^{-1} (representing 10% of the base state shear rate), and for $A = 10^{-7}$, the initial shear rate perturbation is of the order of 10^{-4} (equivalent to 0.01% of the base state shear rate).

It must be noted that the value of $\eta_s = 10^{-4}$ or 10^{-5} is not unrealistic and is possible in an experimental study as shown in Ref. [88]. It is useful to estimate the possible range of Re in shear startup experiments involving wormlike micellar solutions. We assume that the solution density (ρ) is similar to water at room temperature (i.e., 10^3 kg/m^3) and the gap width between the plates or concentric cylinders is approximately 10^{-3} m, the zero shear viscosity of the solution can vary from 10^{-3} Pa s to 10^2 Pa s [26, 34, and 89]. Therefore, Re can be estimated as $U/(\bar{\eta}_s + \bar{\eta}_p)$, where U is the characteristic velocity, and $\bar{\eta}_s$ and $\bar{\eta}_p$ are the solvent and polymer viscosity contribution to the zero shear viscosity of the solution, respectively. The maximum value of Re can be around $10^3 U$, and we can assume a range of Re from 0.1 to 100, which can be achievable in some practical cases depending on the value of U. In the study by Helgeson et al. [26], where steady-state shear banding has been observed using CTAB (Cetyl trimethyl ammonium bromide) solution, the zero shear viscosity is reported to be of the order of 1 Pa s. Therefore, in this case, the value of Re is mainly dependent on U, suggesting that a higher U value will result in a higher Re. Therefore, from the experimental studies reported in the literature, we estimate Re in the range of 0.01 to 100.

The non-linear simulations are carried out using COMSOL 5.0®. The inbuilt partial differential equation solver of COMSOL utilizes the finite element method. The domain (0,1) is discretized into 6452 points. The results for the shear startup of the JS and nRP models converge for 6000 to 10000 domain elements and for a fixed time step ranging between $10^{-5} - 10^{-4}$. The relative and absolute tolerance is kept at 10^{-5} and 10^{-6}, respectively. In this study, we have also verified the numerical solutions with the results reported in the

literature [20 and 76].

III. RESULTS AND DISCUSSION

In our earlier work [44], we demonstrated that if there is a stress overshoot during shear startup, this does not guarantee a positive eigenvalue within the frozen-time linear stability analysis, nor does it necessarily result in the growth of perturbations within the more accurate analysis of linearized dynamics using the fundamental matrix approach. (Some of the caveats of the frozen time analysis have also been discussed in Ref. [20].) The former, in particular, has been used as a signature of transient instability in the literature [20 and 21]. While results from linearized dynamics are valid when the perturbations are infinitesimal, the ultimate answer to the question of whether transient shear banding is present or not must come from fully-nonlinear solutions of shear startup, which is the objective of the present study. Here, we numerically solve the partial differential equations mentioned in Sec. II, and determine the relevance of stress overshoot, positive eigenvalue within a frozen-time stability analysis, and the growth and decay of linearized perturbations on transient shear banding. We analyze the shear startup of JS and nRP models to shear rates in both monotonic and nonmonotonic regions of the constitutive curves as shown in Fig. 1. We revisit the criterion for transient shear banding proposed in Ref. [20] using the JS and nRP models. As the nRP model has also been used in Ref. [20], we use the same parameter values to revisit the shear startup of nRP model.

As discussed in Sec. I, shear banding can be identified and quantified more reliably by the presence of a peak in the second or third derivative of velocity (because the degree of banding metric is not capable of distinguishing between transient inhomogeneities and shear banding) [22–24]. However, in this study, in order to compare our results with those reported in the literature [20 and 21], we calculate the degree of banding to quantify both steady state and transient shear banding in each case. The degree of banding is defined as the difference between the maximum and minimum shear rates of the fluid flow between the parallel plates [20 and 21]. If the degree of shear banding is zero, then the flow is homogeneous otherwise it is inhomogeneous and its magnitude determines the extent of inhomogeneity in the flow. We additionally present the corresponding velocity profiles as a function of time to correlate them with degree of banding for the nRP model.

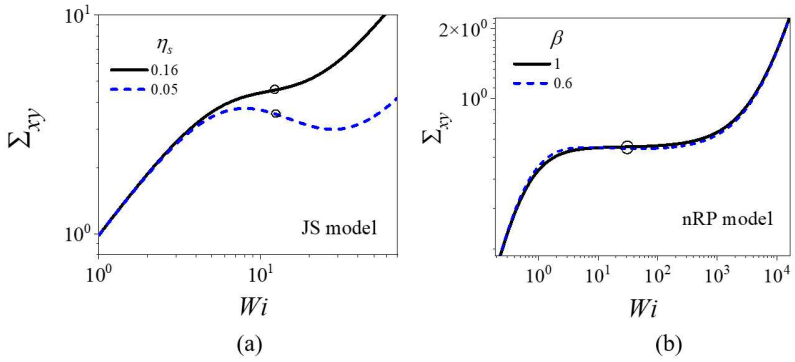

Figure 1. Constitutive curves of (a) JS model and (b) nRP model. The monotonic constitutive curve of JS model is obtained using $\eta_s = 0.16$ and $\xi = 0.01$ and the nonmonotonic constitutive curve is obtained using $\eta_s = 0.05$ and $\xi = 0.01$. The monotonic constitutive curve of nRP model is obtained using $\beta = 1$ and $\eta_s = 10^{-4}$ and the nonmonotonic constitutive curve is obtained using $\beta = 0.6$ and $\eta_s = 10^{-4}$.

We also show the time-dependent evolution of maximum amplitude of linearized perturbation and transient eigenvalue for shear startup of the JS and the nRP model. Some of these results has been published in our earlier study [44], however, these results are included here for comparison of linearized dynamics and nonlinear simulations. Figures 2 and 3 also show time markers to facilitate analysis and compare the shear stress, linearized perturbation, eigenvalue and degree of banding during the shear startup flow.

A. Stress overshoot and transient shear banding

We first study shear startup of the JS model for different initial amplitudes of perturbation, A and Re to examine the sensitivity of transient dynamics on the initial conditions and the value of Re. We fix $\eta_s = 0.16$ and $Wi = 12$ so that the shear rate is in the flatter and monotonic region of the constitutive curve. Figure 2 shows time-dependent evolution of shear stress, linearized perturbation, eigenvalue and degree of banding ($\Delta\dot{\gamma} = \dot{\gamma}_{max} - \dot{\gamma}_{min}$). During shear startup, the shear stress increases, shows an overshoot and then attains a steady state in all the three cases ($A = 10^{-1}$, 10^{-4}, 10^{-7}). We find that shear stress for

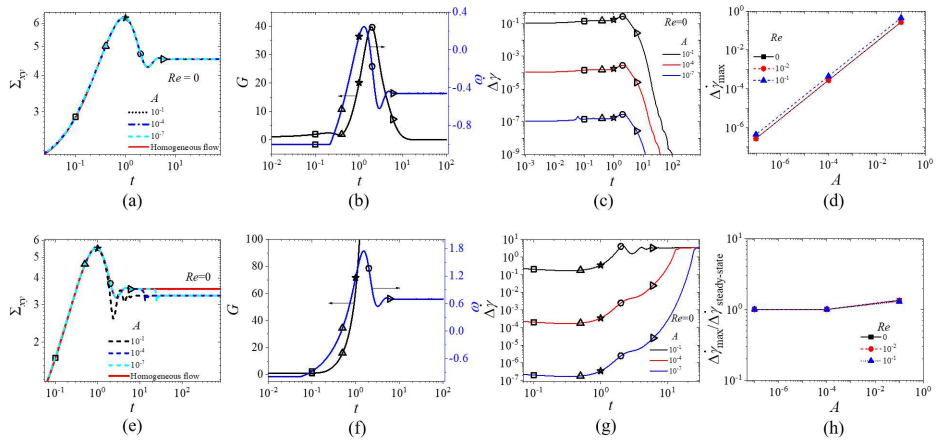

Figure 2. Comparative analysis of shear startup behavior in the monotonic ($\xi = 0.01, \eta_s = 0.16, Wi = 12$) (first row) and nonmonotonic ($\xi = 0.01, \eta_s = 0.05, Wi = 12$) (second row) regions of the constitutive curve. (a) & (e) Shear stress is plotted as a function of time; (b) & (f) the maximum amplitude of linearized perturbation, (G), and eigenvalue (ω) is plotted as a function of time; (c) & (g) degree of banding ($\Delta\dot{\gamma} = \dot{\gamma}_{max} - \dot{\gamma}_{min}$) is plotted as a function of time for different initial amplitude of perturbation, (A); (d) & (h) maximum degree of banding, ($\Delta\dot{\gamma}_{max}$) plotted as a function of initial amplitude of perturbation, (A). The evolution of maximum amplitude of linearized perturbation, and eigenvalue obtained through linear stability analysis, along with the time-dependent evolution of the degree of banding from nonlinear simulations, is depicted for both cases. Markers on plots (a)-(c) and (e)-(g) facilitate correlation of results at specific time points. The effect of the initial amplitude of perturbation and Re on the maximum degree of banding is illustrated for both monotonic and nonmonotonic cases.

all three values of A overlaps for all times and $\Delta\dot{\gamma}$ is initially of the order of A before finally decaying to zero. These results show that an imposition of perturbations with initial amplitude A engenders a response which is only commensurate with the forcing, and this response cannot be interpreted as a signature of a transient (elastic) instability. For the results shown in Fig. 2(c), the system is merely adjusting itself to the imposed perturbation before reaching the homogeneous steady state. Therefore, on this count, Fig. 2 clearly shows that there is no instability in the JS model from nonlinear simulations.

In Fig. 2(b), we observe a transient growth of linearized perturbations followed by their subsequent decay and a transiently positive eigenvalue during shear startup of JS model for the monotonic case (see Appendix). Interestingly, despite the presence of a transiently positive eigenvalue and the growth of linearized perturbations, nonlinear simulations of the JS model do not reveal any significant growth in the degree of banding (Fig. 2(c)). These findings suggest that the nonlinearities inherent in the JS model have a stabilizing effect during shear startup. Also, Fig. 2(d) shows that the maximum degree of banding ($\Delta\dot{\gamma}_{max}$) to be of the order of A and is independent of Re.

We next study the shear startup flow of the JS model for the case when the shear rate is in the nonmonotonic region of the constitutive curve and steady state shear banding is observed. We find that the shear stress increases and shows an overshoot before attaining steady state. The stress evolution data overlaps with each other in all these cases ($A = 10^{-1}$, 10^{-4}, 10^{-7}), except just before attaining a final steady-state stress. We find that the time of attaining steady state value of degree of banding ($\Delta\dot{\gamma}$) depends on the value of A. Higher the value of A, lower is the time required for the JS model to become unstable and attain steady state shear banding as shown in Fig. 2(g). Also, there is no pronounced transient increase (i.e., $\Delta\dot{\gamma}$ is not significantly greater than $\Delta\dot{\gamma}_{steady-state}$) during the time range in which there is a stress decay after overshoot as shown in Fig. 2(e). During shear startup at $Wi = 12$ in the nonmonotonic region of the constitutive curve, the time at which degree of banding increases, and the time of stress overshoot may seem to be close to each other (time of increase in degree of banding$= 0.3$, time of stress overshoot$= 1$). However, for $Wi = 27$, we find that the time of degree of banding increase occurs almost at the beginning of the flow, while the time of stress overshoot is significantly delayed (time of increase in degree of banding$= 0.0004$, time of stress overshoot$= 0.41$; data not shown). This result further emphasizes that stress overshoot may not have any correlation with onset of banding during shear startup of JS model with shear rate in the nonmonotonic region of the constitutive curve.

The above results show that during the time evolution of shear startup flow, growth rate of linearized perturbations diverges, but the degree of banding remains finite. In addition, the ratio of $\Delta\dot{\gamma}_{steady-state}$ and $\Delta\dot{\gamma}_{max}$ is independent of Re. Therefore, for both monotonic and nonmonotonic cases, in the presence of stress overshoot, JS model shows (i) no transient shear banding even though the linearized perturbation show growth and decay during the

flow, (ii) the maximum value of degree of banding ($\Delta\dot{\gamma}_{max}$) is of the order of A and varies in a linear manner with A, and is also independent of Re, (iii) the time associated with maximum degree of banding depends on A. Even if the shear rate is in the nonmonotonic region of the constitutive curve, distinct transient shear banding is not observed and increase in degree of banding begins almost at beginning of the flow and this time is much lower than the time at which shear stress decreases after its overshoot.

We next study the shear start-up of the nRP model when the shear rate is in the monotonic region of the constitutive curve as shown in Fig. 3. The shear start-up of the nRP model under the creeping-flow assumption when the shear rate is in the monotonic region of the constitutive curve ($Wi = 30$, $\eta_s = 10^{-4}$, $A = 10^{-1}$ and $\beta = 1$) has been reported by Moorcroft and Fielding [20]. We have recomputed and included this result for comparison purposes.

We examine if the transient dynamics is sensitive to the initial condition and value of Re. At first, we find that shear stress evolution does not overlap with each other for different values of initial amplitude of perturbation ($A = 10^{-1}$, 10^{-4}, and 10^{-7}) at $Re = 0$ as shown in Fig. 3(a). The velocity profiles during shear startup flow for $A = 10^{-1}$ and $Re = 0$ show the presence of transient shear banding with a negative velocity profile as shown in Fig. 4(a). The corresponding evolution of degree of banding on a linear-log plot is shown in Fig. 3(c). The evolution of $\Delta\dot{\gamma}$ as a function of time shows a sharp increase and then finally decays to zero. The inset of Fig. 3(c) (left side) shows the early time behavior ($t = 0 - 0.3$) on a log-linear plot (of degree of banding versus time) and right inset of Fig. 3(c) shows the evolution only for $A = 10^{-4}$ and $t = 0 - 0.01$. The data for degree of banding increases linearly followed by a growth which is stronger than linear before final decay to zero on a log-linear plot (of degree of banding time). Therefore, the linear increase in the data on a log-linear plot (Fig. 3(c)) shows that the growth of perturbation is exponential which implies that the shear startup of nRP is transiently (and linearly) unstable for $Re = 0$. However, the exponential growth of perturbation begins almost at the start of the flow (refer to the square symbol time marker in Figs. 3(a-c) and its inset) and may not have any correlation with time at which shear stress starts to decrease after its overshoot. Similarly, the value of $\Delta\dot{\gamma}_{max}$ is significantly larger than the input amplitude A as shown in Fig. 3(d). Therefore, we can treat this as an intrinsic instability of shear startup of the nRP model.

Furthermore, in Fig. 3(b) we observe a transiently high growth of linearized perturbations

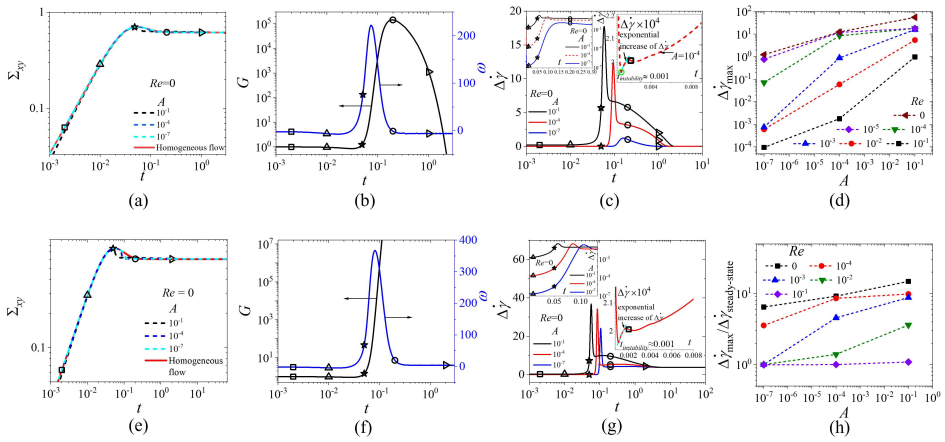

Figure 3. Comparative analysis of shear startup behavior in the monotonic ($\beta = 1$, $\eta_s = 10^{-4}$, $Wi = 30$) (first row) and nonmonotonic ($\beta = 0.6$, $\eta_s = 10^{-4}$, $Wi = 30$) (second row) regions of the constitutive curve of nRP model. (a) & (e) Shear stress is plotted as a function of time; (b) & (f) the maximum amplitude of linearized perturbation, (G), and eigenvalue (ω) is plotted as a function of time; (c) & (g) degree of banding ($\Delta\dot{\gamma} = \dot{\gamma}_{max} - \dot{\gamma}_{min}$) is plotted as a function of time for different initial amplitude of perturbation, (A); (d) & (h) maximum degree of banding, ($\Delta\dot{\gamma}_{max}$) plotted as a function of initial amplitude of perturbation, (A). The evolution of maximum amplitude of linearized perturbation and eigenvalue obtained through linear stability analysis, along with the time-dependent evolution of the degree of banding from nonlinear simulations, is depicted for both cases. Markers on plots (a)-(c) and (e)-(g) facilitate correlation of results at specific time points. The effect of the initial amplitude of perturbation and Re on the maximum degree of banding is illustrated for both monotonic and nonmonotonic cases.(Some of the results presented in Figures (a)-(c) and (e)-(g) have previously been demonstrated by Moorcroft and Fielding [20]. However, in this study, we have recalculated and included these results to facilitate a comprehensive comparison.)

which is of the order of 10^4 followed by their subsequent decay and a transiently positive eigenvalue during shear startup of nRP model at $Wi = 30$, $\eta_s = 10^{-4}$, and $\beta = 1$. However, nonlinear simulations of the nRP model do not show a high growth in the degree of banding (Fig. 3(c)). These findings suggest that the nonlinearities inherent in the nRP model have

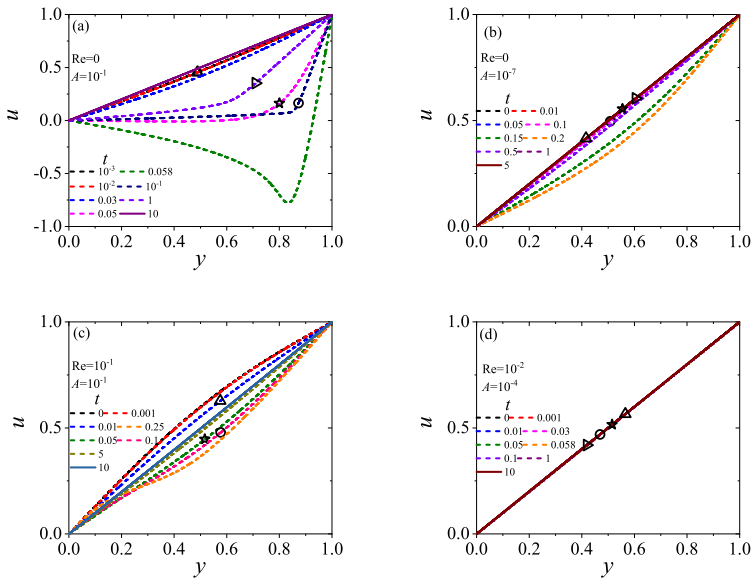

Figure 4. Velocity profile evolution during the shear startup flow of the nRP model fluid at $Wi = 30$, $\eta_s = 10^{-4}$, and $\beta = 1$ which corresponds to a shear rate in the monotonic region of the constitutive curve. Figure (a) shows result for $Re = 0$ and $A = 10^{-1}$ and figure (b) shows result for $A = 10^{-7}$ and $Re = 0$. Figure (c) shows result for $A = 10^{-1}$ and $Re = 10^{-1}$ and figure (d) shows result for $A = 10^{-4}$ and $Re = 10^{-1}$. Markers in figures (a)-(d) facilitate correlation of results at specific time points with results shown in Figs.3(a)-(c). (The results presented in Figure (a) have previously been demonstrated by Moorcroft and Fielding [20]. However, in this study, we have recalculated and included these results to facilitate a comprehensive comparison.)

a stabilizing effect during shear startup.

Figure 3(c) shows that the time of peak of $\Delta\dot{\gamma}$ decreases with increase in value of A and the value of $\Delta\dot{\gamma}_{max}$ also depends on the value of A. On increasing the value of A, the value of $\Delta\dot{\gamma}_{max}$ also increases but not in a linear manner as shown in Fig. 3(d). The effect of decrease in initial amplitude of perturbation is also evident in Fig. 4(b) wherein no transiently negative velocity profile is observed and extent of transient inhomogeneity is comparatively lesser than that is observed at high initial amplitude of perturbation in Fig. 4(a). We also find

that for $Re \neq 0$, $\Delta\dot{\gamma}_{max}$ decreases significantly and is negligible for $Re = 0.1$ as shown in Fig. 3(d) and in the simulataneous velocity profiles (Figs. 4(d) and 4(c)). In these figures, it is evident that with inclusion of non-zero Re, the transient inhomogeneities are negligible and velocity profile is almost linear at all values of time even at low value of $\eta_s = 10^{-4}$. The effect of Re on shear startup of nRP model is discussed in detail in Sec. III B.

The shear stress, eigenvalue, degree of banding and velocity profile obtained using $Wi = 30$, $\eta_s = 10^{-4}$, $\beta = 1$, $A = 10^{-1}$, and $Re = 0$ in Figs. 3(a)-(c) and 4(a) has also appeared in Ref. [20]. We have included these results only for comparison purposes.

We also check the sensitivity of the transient dynamics on initial conditions of shear startup of nRP model for the nonmonotonic case. We find that, if the shear rate is in the nonmonotonic region of the constitutive curve, the shear stress evolution as a function of time for different values of A does not overlap as also observed in the previous case (the initial shear rate perturbation and shear stress perturbation is the same as the previous case i.e., shear startup of nRP model with shear rate in the monotonic region of the constitutive curve, as the value of A, η_s, and Wi is same in this case as well). If the value of A is higher, shear stress attains steady state at lower values of time as shown in Fig. 3(e). The evolution of $\Delta\dot{\gamma}$ with time also confirms that the degree of banding shows a rapid increase to attain a maximum value and then decreases to a constant value on a linear-log plot of $\Delta\dot{\gamma}$ versus time (Fig. 3(g)). If $\Delta\dot{\gamma}$ versus time is plotted on a log-linear scale, then it becomes clear that the increase in degree of banding is linear or stronger than linear before attaining a steady state as shown in the insets of Fig. 3(g). This result demonstrates the exponential growth of perturbations which is in agreement with criterion of Yerushalmi et al. [25]. However, the time at which degree of banding begins to grow exponentially is much lesser than time at which shear stress starts to decrease after its overshoot. In the literature [34, 35, 46–48, and 60], the time of decrease in stress after stress overshoot is often linked with time at which steady state shear banding structure begins to form. However, our results show that shear banding structures starts to form at much earlier times, but may not be discernible in experiments, and hence the shear banding structures may not be associated with the time of decrease in stress after its overshoot.

More importantly, the evolution of $\Delta\dot{\gamma}$ with time on a log-linear plot, for the nRP model shows a linear increase initially followed by a nonlinear increase in both cases of shear rate in the monotonic as well as nonmonotonic region of the constitutive curve (Figs. 3(c) and

3(g)). Because of these findings, it is clear that the linear stability analysis predicts only the exponential growth at very early times, and soon after nonlinear effects take over, and hence the linearized dynamics loses its relevance for times where there is a stress overshoot and decay. The caution regarding the use of linear stability analysis in unsteady flow (shear startup flow) to assess the occurrence of shear banding has also been pointed out by Peterson [63].

The transiently high value of $\Delta\dot{\gamma}$ shows the presence of strong transient inhomogeneities and the constant value of $\Delta\dot{\gamma}$ at steady state indicates the presence of steady state shear banding. Figure 3(h) shows that for $Re = 0$, the value of $\Delta\dot{\gamma}_{max}$ is much higher than $\Delta\dot{\gamma}_{steady-state}$, however, $\Delta\dot{\gamma}_{max}$ depends on the value of A but not in a linear fashion. Furthermore, the ratio of $\Delta\dot{\gamma}_{max}$ and $\Delta\dot{\gamma}_{steady-state}$ decreases with increase in Re which suggests the decrease in sharp transient inhomogeneity with increase in Re. The high ratio of $\Delta\dot{\gamma}_{max}$ and $\Delta\dot{\gamma}_{steady-state}$ highlights the transient inhomogeneities that are not part of gradual development of steady state shear banding.

The sensitivity of the transient dynamics (or $\Delta\dot{\gamma}_{max}$) during the shear startup of the nRP model to the initial amplitude of perturbation (A) and Re emphasizes how transient inhomogeneities are influenced by the specified conditions which is also in agreement with observations of Ref. [21]. This observation implies that these transient inhomogeneities may not constitute genuine transient instabilities, and are unlike the the inherent instability seeen in steady-state shear banding.

The contrasting results of the JS and nRP models can be ascribed to the coupled effects of value of initial amplitude of perturbation, η_s and Re. First we discuss the effect of initial amplitude of perturbation and the effect of value of η_s and Re on shear startup dynamics is discussed in Sec. III B. In the case of JS model, the magnitude of the initial shear rate perturbation is not unrealistically high because the value of η_s was not much smaller compared to unity. In the case of nRP model, the initial shear rate perturbation becomes unrealistic because of low value of η_s if the stress perturbations are $O(1)$. Therefore, under the creeping-flow assumption, if the initial shear rate perturbation is realistic then there may be no transient shear banding observed in shear startup flow of JS and nRP models. (The change in value of initial shear rate perturbation with η_s for different cases considered in Figs. 2 and 3 is discussed in Sec. II.)

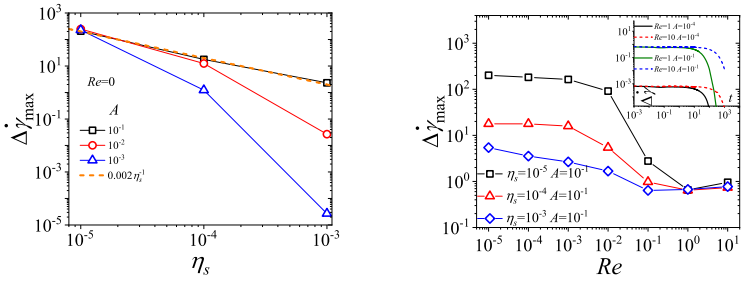

(a) (b)

Figure 5. (a)Variation of maximum of degree of banding during the shear startup flow as a function of η_s during shear startup flow of the nRP model fluid for $Wi = 30$, and $\beta = 1$. These results are obtained for $Re = 0$. (b) Variation of maximum of degree of banding ($\Delta\dot{\gamma}_{max}$) during the shear startup as a function of Re for the nRP model for $Wi = 30$, $\beta = 1$. Here, $A = 10^{-1}$, and $\eta_s = 10^{-3}$, 10^{-4}, and 10^{-5}. The inset shows the evolution of degree of banding ($\Delta\dot{\gamma} = \dot{\gamma}_{max} - \dot{\gamma}_{min}$) with time for the nRP model for $\eta_s = 10^{-4}$. Here, $Re = 1$, 10 and $A = 10^{-1}$, 10^{-4}

B. Effect of solvent viscosity ratio and *Re*

It has been reported in literature that decrease in η_s leads to more flattening of the constitutive curve for both JS and nRP models (see Fig. 1 of Ref. [44], and Refs. [20 and 21]). The flatness of the constitutive curve can also be increased by increasing the number of entanglements [35]; however, in this study, we focus only on the effect of η_s. Several results have been reported in the literature [20 and 21] suggesting that increasing the flatness of constitutive curve can affect the occurrence of transient shear banding in shear startup flow. In this section, we focus on the effect of solvent viscosity (and, thence, the flatness of the constitutive curve), only for shear rates in the monotonic region of the constitutive curve. In our previous study [44], we showed using the JS model that there is no significant change in the transiently maximum eigenvalue or the maximum value of growth of linearized perturbation with decrease in η_s. Note that the value of η_s cannot be lowered below $1/9$ in order for the constitutive curve to be monotonic. During the course of the present study, we found that even in the nonlinear simulations, there is no significant effect of decreasing the solvent viscosity (from 0.16 to 0.115) on degree of banding evolution (data not shown). We

defer the start-up to nonmonotonic regions with regard to the role of η_s to a future study.

For the nRP model, we found that there is a significant change in the transiently maximum eigenvalue or the maximum value of growth of linearized perturbation with decrease in η_s [44]. In this study, using nonlinear simulations, we observed that as η_s decreases, $\Delta\dot{\gamma}_{max}$ shows a steep increase for various initial amplitudes of perturbation (refer to Fig. 5(a)). Furthermore, for very low η_s (i.e., 10^{-5}), the peak of the degree of banding becomes independent of the initial amplitude of perturbation for values of A and Wi explored. This finding underscores the consistency between linearized dynamics and nonlinear simulation results. Our previous study also showed that introducing a nonzero Re resolves the issue of the divergence of the transient maximum eigenvalue. Instead of divergence, the transient maximum eigenvalues remain bounded at low η_s, and this constant value decreases with an increase in Re (see Fig. 13 of Ref. [44]). In our nonlinear simulations, we found complete alignment with linearized dynamics for non-zero Re, the divergence of $\Delta\dot{\gamma}_{max}$ with a decrease in η_s transforms into a constant value as η_s decreases (refer to Fig. 5(b)).

Another compelling indication of unrealistic results at low η_s, and the mitigation of these issues by introducing a finite Re, can be observed in the evolution of the velocity profile over time during the shear startup of the nRP model at $\eta_s = 10^{-5}$ (Fig. 6(a)). For $Re = 0$, the velocity profile deviates from the linear profile and exhibits transient negative velocities, with the most extreme local velocity reaching -15 This implies that if the top plate velocity is 1, the local velocity of the fluid between the plates is 15 times the top plate velocity in the opposite direction. Therefore, the unrealistic nature of results obtained due to the low value of η_s, even with $A = 10^{-7}$, and is consistent with the unbounded growth of linearized perturbations shown in our previous study [44]. Interestingly, for $Re = 0.1$, the velocity profile remains linear at all times, and no transient inhomogeneity is observed (see Fig. 6(b)).

It is useful to contrast the large transiently negative velocity profiles (discussed above) with experimental shear startup results. Recently, Rassolov and Mohammadigoushki [35] obtained velocity profile evolution for wormlike micellar solution during shear startup flow and they found that steady state is banded. During the evolution to steady state, the velocity of fluid between two plates attains a negative velocity; whose magnitude is at most 25% of the top plate velocity. However, the maximum magnitude of negative velocity of fluid between plates obtained for $\eta_s = 10^{-4}$ (when shear rate is in the nonmonotonic region for

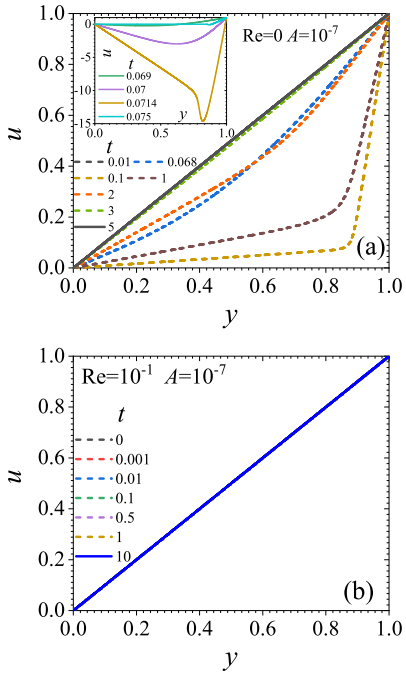

Figure 6. Velocity profile evolution during the shear startup flow of the nRP model at $Wi = 30$, $\eta_s = 10^{-5}$, and $\beta = 1$ which corresponds to a shear rate in the monotonic region of the constitutive curve. Figure (a) shows result for $Re = 0$ and $A = 10^{-7}$ and figure (b) shows result for $A = 10^{-7}$ and $Re = 10^{-1}$.

the nRP model) can be at most 300% of the top plate velocity (as shown in Ref. [20]), which is far greater in magnitude as compared to 25% of top plate negative velocity observed experimentally [35]. Similarly, Boukany and Wang performed shear startup of entangled wormlike micellar solutions and showed that the transient local velocity in the opposite direction can be at most 0.8-30% of the top plate velocity [56]. It has been observed in literature [20 and 21] that the maximum magnitude of negative velocity during shear startup, if shear rate is in monotonic region of constitutive curve, is lesser than that when the shear rate is in the nonmonotonic region of constitutive curve. Therefore, based on our results we

conjecture that either transient negative velocity will not be observed during experiments if shear startup is performed with shear rate in monotonic region of the constitutive curve or the maximum magnitude of negative transient velocity profile will be much lesser than 100% or 1500% of the top plate velocity that has been predicted by nRP model in Figs. 4(a) and 6. The comparison with experimental results further highlights the importance of non-zero Re during shear startup of nRP model which can help in regularising the results.

Next, we examine the effect of further increasing Re (i.e. $Re > 0.1$) at low η_s. It is observed that for $Re \leq 0.1$, the degree of banding is not of the order of the initial amplitude of perturbation (A), and its value is significantly higher during the shear startup of the nRP model for the monotonic case (see Fig. 3(c)). However, for $Re = 1$ and $Re = 10$, the variation of the degree of banding $\Delta\dot{\gamma}$ with time is of the order of the initial amplitude of perturbation (A), as shown in the inset of Fig. 5(b). For the JS model, we have observed that the degree of banding $\Delta\dot{\gamma}$ with time is of the order of the initial amplitude of perturbation (A) (see Fig. 2(c)), where no transient inhomogeneity is observed even for $Re = 0$.

In Sec. II, we raised a question about the validity of the creeping-flow assumption in solving the nRP model for $\eta_s \ll 1$. There are two broad reasons as to why the creeping-flow assumption for $\eta_s \ll 1$ might lead to erroneous results in the numerical solution: (i) the transient maximum eigenvalue or transient growth rate diverges with decrease in η_s suggesting that transient growth of perturbations in nonlinear simulations can also diverge. However, if the transient growth rate of shear rate perturbation diverges, the creeping-flow assumption cannot hold true. This is because, while neglecting the acceleration term in the Cauchy momentum equation, on account of it being multiplied by Re, it is implicitly assumed that for $Re \ll 1$, the acceleration term must remain finite. However, when the perturbation growth diverges, the acceleration terms also exhibit a similar behavior, and the product of Re and du/dt can no longer be neglected. (ii) Due to the creeping-flow assumption, the initial shear rate perturbation cannot be specified directly and it is of the order of $\frac{\sigma_{xy}}{\eta_s Wi}$ which results in imposing unrealistic magnitudes of initial shear rate perturbation, especially when the initial stress perturbations are kept $O(1)$. Alternatively, these unrealistic results may also be averted by inclusion of stretching and solving the shear startup of Rolie Poly model at very low values of η_s [20 and 21].

It is important to note that after inclusion of nonzero Re, if the solvent viscosity contribution is very low such that $\eta_s \leq O(10^{-4})$, then even with direct imposition of realistic shear

rate perturbation, perturbations may eventually reach very high magnitudes. Figure 5(b) shows that beyond a critical Re, the perturbations do not grow unbounded during shear startup of the nRP model.

The above results show that if η_s is $O(10^{-3} - 10^{-1})$, then $\Delta\dot{\gamma}_{max}$ is of the order of A for $Re = 0$ and $Re \neq 0$. If η_s is $O(10^{-4})$, then $\Delta\dot{\gamma}_{max}$ is very sensitive to the value of A under the creeping-flow assumption, and is also affected by inclusion of inertial effects. For $\eta_s = 10^{-5}$, the change in initial amplitude of perturbation does not affect $\Delta\dot{\gamma}_{max}$ and it is only affected by inclusion of nonzero Re. The fact that the velocity profiles during transient evolution can be so sensitive to Re, when η_s is very small, suggests that the specific details of the experimental conditions will likely play a crucial role in the nature of the observed velocity profiles during shear startup.

C. Effect of initial condition on transient inhomogeneities

We have also investigated the shear startup of JS and nRP models by utilising random noise as the initial condition (see Eq. 15). This approach ensures that the results obtained are independent of any specific initial condition. Our findings indicate that, for the JS model, the velocity profile remains linear at all times, with no transient inhomogeneities (data not shown). This behavior is consistent with that obtained using sinusoidal initial conditions.

However, for nRP model, we find that that the transient evolution is sensitive to different initial conditions when using two distinct random noise inputs. Subsequently, the velocity profile becomes linear after the introduction of random noise, but transient inhomogeneities emerge at different times for different random noise inputs (see Figs. 7(a) and 7(b)). These complex transient inhomogeneities also demonstrate the possibility of temporary negative local velocities.

In the first case (Fig. 7(a)), we observe the formation of two distinct shear rate bands at $t = 0.2$ and 0.7 due to the complex transient inhomogeneities. However, in the second case (Fig. 7(b)), these inhomogeneities do not evolve into separate bands with distinct shear rates. The velocity profile becomes linear at $t = 1.5$ in the first case, while in the second case, it becomes linear at $t = 3$. Therefore, the transient evolution of the velocity profile appears to be sensitive to the initial conditions. It is useful to point out that the earlier effort

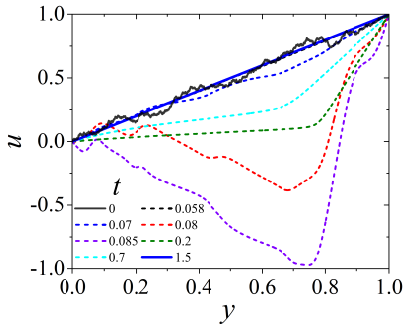

(a)

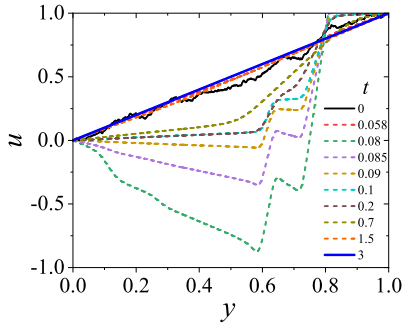

(b)

Figure 7. Velocity profile evolution during shear startup of the nRP model with shear rate in the monotonic region of the constitutive curve ($Wi = 30$, $\eta_s = 10^{-4}$, $A = 10^{-1}$, $Re = 0$, $\beta = 1$) for two different random noise (with zero mean) as initial conditions is shown in (a) and (b).

of Moorcroft and Fielding [20] used a noisy sinusoidal initial condition (see their Fig. 14), while we use a pure white noise with zero mean. The results of Ref. [20] closely resemble our results obtained for a purely sinusoidal initial condition (without any noise, see Fig. 4(a)), and are quite different from those obtained using a pure white noise (with zero mean) shown in Fig. 7. Thus, the transient inhomogeneities and shear banding seen in the numerical simulations are rather sensitive to the nature of the initial conditions.

IV. CONCLUSION

We presented results from nonlinear simulations of shear startup using the JS and nRP models, to understand the importance and relevance of transient shear banding in this flow protocol. We compared earlier results from linearized dynamics [44] with the present nonlinear results in order to examine the extent of validity of the former. We find that stress overshoot during shear startup does not necessarily result in transient banding, regardless of whether the applied shear rates is in the monotonic or nonmonotonic regions of the constitutive curve. Our nonlinear simulations reveal that transient shear banding is absent during shear startup of the JS model for the parameter regimes explored. For the nRP model, however, under the restricted parameter regimes of very low values of solvent to solution viscosity ($\sim O(10^{-4})$) and in the absence of inertia, we find significant increase in degree of banding before the steady state is reached. We also showed that for the nRP model, the initial exponential growth of degree of banding has no relation with the time at which stress decreases after its overshoot, regardless of whether the startup is to shear rates in the monotonic or nonmonotonic regions of the constitutive curve.

In the inertialess limit, however, the initial shear rate perturbation cannot be prescribed and its magnitude is instead governed by the initial amplitude of the σ_{xy} stress perturbation and η_s. Consequently, the results for shear startup of the nRP model show a nonlinear dependence on initial amplitude of perturbations and a discernible transient shear banding is observed only if $\eta_s < 10^{-3}$ and if the initial shear rate perturbations are unrealistically high for shear rates in the monotonic region of the constitutive curve. For the JS model, we found that the maximum of degree of banding is proportional to the initial amplitude of perturbations, even for a six-fold increase in their order of magnitude, suggesting that there is no intrinsic transient instability in the JS model during shear startup. We also studied shear startup of both JS and nRP models by including inertial effects so that initial shear rate perturbation can be specified directly. The results of JS model again showed a linear dependence for the variation of maximum of degree of banding with initial amplitude of perturbation, even in the presence of inertial effects. However, for the nRP model, the maximum of degree of banding showed linear dependence on initial amplitude of perturbation only beyond a threshold level of fluid inertia. This critical magnitude of Re increases with decrease in η_s. Furthermore, our findings demonstrated that the stabilizing effect of

inertia occurs when the transient growth of perturbations is significantly high. The occurrence of transient inhomogeneities during shear startup in nonlinear simulations might be a consequence of the use of the creeping-flow assumption, in regimes where the assumption is not self-consistent. In the absence of inertia, we also showed that maximum of degree of banding diverges with a power law exponent of -1 on decreasing η_s. There is no divergence of maximum of degree of banding on decreasing η_s when inertial effects are included.

Additionally, we investigated the influence of the initial condition on the shear startup of the nRP model with shear rate in the monotonic region of the constitutive curve by employing random noise (with zero mean) as the initial condition. Our findings revealed that the transient dynamics of the shear startup flow are highly sensitive to the initial condition. Instead of observing clear transient shear banding, we observed the emergence of complex transient inhomogeneities that are contingent upon the specific realization of the inital random noise. This suggests that the transient shear banding reported for shear startup using the nRP model using a sinusoidal initial perturbation could be a consequence of this specific initial condition, and hence its relevance to real experimental observations need to be evaluated carefully.

The comparison of results obtained using the fundamental matrix method for linearized evolution of perturbations and those from nonlinear simulations showed that nonlinear terms mitigate the divergence of perturbations for both JS and nRP models. The results obtained using different initial amplitude of perturbations showed that the time associated with maximum value of degree of banding and the maximum value of degree of banding depends on the initial amplitude of perturbation. On the basis of these two observations, we conclude that occurrence of transient shear banding, if any, is not always triggered by a linear instability, and is governed by the following factors: (1) the initial amplitude of perturbation, (2) the solvent to solution viscosity ratio η_s, and (3) the inertial effects characterized by Re. Overall, we show that the results of shear startup of nRP model are very sensitive to initial amplitude of perturbations and the magnitude of inertial effects if $\eta_s \ll 1$. Therefore, there will not be any transient shear banding in shear startup of JS and nRP models if (i) $\eta_s > 10^{-3}$, (ii) inertial effects are included if $\eta_s \ll 1$, because of very high transient growth of perturbations, creeping-flow assumption is not self consistent, and (iii) realistic initial amplitude of perturbation is imposed if $\eta_s \ll 1$, within the creeping-flow assumption. More importantly, the comparison of linear and nonlinear studies showed that growth of per-

turbations as indicated by linearized dynamics may not necessarily signify transient shear banding in the nonlinear simulations. The results from both JS and nRP models show that the ultimate answer to whether there will be any transient shear banding or not can be ascertained only using nonlinear simulations.

ACKNOWLEDGMENT

We acknowledge financial support from the Science and Engineering Research Board, Government of India.

DATA AVAILABILITY

The data that supports the findings of this study are available within the article. Additional data are available from the corresponding author upon reasonable request.

APPENDIX

A. Linearized analysis

In Figs. 2(b) and 3(c), two key parameters are used to assess the linearized transient stability of the system: the transient maximum eigenvalue $\boldsymbol{\omega}$ and the growth of linearized perturbations $G(t)$.

First, the eigenvalue $\boldsymbol{\omega}$ is determined through a linear stability analysis, where we linearize the governing equations around the time-dependent base state [44]. At each instant in time, a modal stability analysis is performed to calculate $\boldsymbol{\omega}$, which characterizes the exponential growth or decay of perturbations. In this case, the eigenvalue $\boldsymbol{\omega}$ is a function of time and indicates whether the flow is unstable (when $\boldsymbol{\omega}$ has a positive real part) or stable (when $\boldsymbol{\omega}$ has a negative real part). However, it is important to note that the accuracy of this "frozen-time" analysis depends on the relative rates of perturbation growth and base state evolution.

We also calculate the growth coefficient $G(t)$, which measures the maximum amplification of perturbations over time. The growth coefficient $G(t)$ is defined as:

$$G(t) = \lim_{\underset{\sim}{x}(0)\neq 0} \sup \frac{|\underset{\sim}{x}(t)|}{|\underset{\sim}{x}(0)|}$$

where $G(t)$ is the growth coefficient at time t, $\underset{\sim}{x}(t)$ represents the vector of the perturbations at time t, and $\underset{\sim}{x}(0)$ is the initial vector of the perturbations. To compute $G(t)$, we express the evolution of the perturbations using the fundamental matrix $\underset{\approx}{Y}(t)$, such that:

$$\underset{\sim}{x}(t) = \underset{\approx}{Y}(t)\underset{\sim}{x}(0)$$

where $\underset{\approx}{Y}(t)$ is the fundamental matrix describing the time evolution of the perturbations. Substituting this into the expression for $G(t)$, we obtain:

$$G(t) = ||\underset{\approx}{Y}(t)||$$

where $||\underset{\approx}{Y}(t)||$ is the norm of the fundamental matrix $\underset{\approx}{Y}(t)$. Here, $G(t)$ captures the maximum possible growth of perturbations as governed by $\underset{\approx}{Y}(t)$. For further details, readers are advised to refer to our earlier study (Ref. [44]).

B. Shear startup of JS model

The evolution of velocity profile during shear startup of JS model pertaining to results shown in Fig. 2 is presented below as Fig. A1.

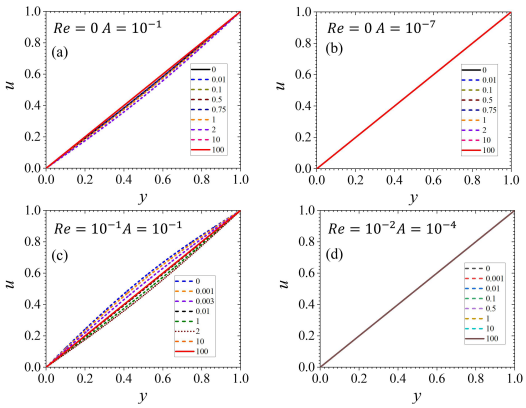

Figure A1. Velocity profile evolution during shear startup of the JS model with shear rate in the monotonic region of the constitutive curve ($Wi = 12$, $\eta_s = 0.16$, $\xi = 0.01$) for different initial amplitude of perturbation, A and Re. (a) $Re = 0$ and $A = 10^{-1}$ (b) $Re = 0$ and $A = 10^{-7}$ (c) $Re = 10^{-1}$ and $A = 10^{-1}$ (d) $Re = 10^{-2}$ and $A = 10^{-4}$

REFERENCES

[1]M. M. Denn, "Extrusion instabilities and wall slip," Annual Review of Fluid Mechanics **33**, 265–287 (2001).

[2]Y. M. Joshi, A. K. Lele, and R. Mashelkar, "Slipping fluids: a unified transient network model," Journal of Non-Newtonian Fluid Mechanics **89**, 303–335 (2000).

[3]C. J. Petrie and M. M. Denn, "Instabilities in polymer processing," AIChE Journal **22**, 209–236 (1976).

[4]E. Howells and J. Benbow, "Flow defects in polymer melts," Trans. Plast. Inst **30**, 240–253 (1962).

[5]Y. M. Joshi and M. M. Denn, "Planar contraction flow with a slip boundary condition," Journal of Non-Newtonian Fluid Mechanics **114**, 185–195 (2003).

[6]Y. M. Joshi and M. M. Denn, "Rupture of entangled polymeric liquids in elongational flow with dissipation," Journal of Rheology **48**, 591–598 (2004).

[7]E. S. G. Shaqfeh, "Purely elastic instabilities in viscometric flows," Annual Review of Fluid Mechanics **28**, 129–185 (1996).

[8]T. C. Kumawat, "Thin film flow inside a uniformly heated/cooled inclined rotating cylinder," Physics of Fluids **36** (2024).

[9]Z. Xiong, P. Angerman, M. Ellero, B. Sandnes, and R. Seto, "Ridge instability in dense suspensions caused by the second normal stress difference," Physics of Fluids **36** (2024).

[10]M. Davoodi, K. Zografos, P. Oliveira, and R. Poole, "On the similarities between the simplified phan-thien–tanner model and the finitely extensible nonlinear elastic dumbbell (peterlin closure) model in simple and complex flows," Physics of Fluids **34** (2022).

[11]L. Liu, "Matched asymptotic analysis of steady viscoelastic wake flows," Physics of Fluids **34** (2022).

[12]E. Gryparis and G. C. Georgiou, "Annular poiseuille flow of bingham fluids with wall slip," Physics of Fluids **34** (2022).

[13]C. Balan, "Note on the start-up of couette flow for viscoelastic fluids," Physics of Fluids **35** (2023).

[14]C. Sasmal, "Effect of micelle breaking rate and wall slip on unsteady motion past a sphere translating steadily in wormlike micellar solutions," Physics of Fluids **34** (2022).

[15]M. B. Khan and C. Sasmal, "Effect of micelle breakage rate on flows of wormlike micellar solutions through pore throats," Journal of Non-Newtonian Fluid Mechanics **307**, 104853 (2022).

[16]F. Hamid, C. Sasmal, and R. Chhabra, "Dynamic mode decomposition analysis and fluid-mechanical aspects of viscoelastic fluid flows past a cylinder in laminar vortex shedding regime," Physics of Fluids **34** (2022).

[17]S. Jamali, A. Boromand, N. Wagner, and J. Maia, "Microstructure and rheology of soft to rigid shear-thickening colloidal suspensions," Journal of Rheology **59**, 1377–1395 (2015).

[18]A. Singh, R. Mari, M. M. Denn, and J. F. Morris, "A constitutive model for simple shear of dense frictional suspensions," Journal of Rheology **62**, 457–468 (2018).

[19]M. Singh, R. Ragoju, G. Shiva Kumar Reddy, and C. Subramani, "Predicting the effect of inertia, rotation, and magnetic field on the onset of convection in a bidispersive porous medium using machine learning techniques," Physics of Fluids **35** (2023).

[20]R. L. Moorcroft and S. M. Fielding, "Shear banding in time-dependent flows of polymers and wormlike micelles," Journal of Rheology **58**, 103–147 (2014).

[21]J. Adams, S. M. Fielding, and P. D. Olmsted, "Transient shear banding in entangled polymers: A study using the rolie-poly model," Journal of Rheology **55**, 1007–1032 (2011).

[22]A. Jain, R. Singh, L. Kushwaha, V. Shankar, and Y. M. Joshi, "Role of inertia and thixotropy in start-up flows of aging soft materials: Transient dynamics and shear banding in a rate-controlled flow field," Journal of Rheology **62**, 1001–1016 (2018).

[23]L. Kushwaha, V. Shankar, and Y. M. Joshi, "Dynamics and shear banding in stress-controlled start-up shear flow of a model aging soft materials: the role of inertia and thixotropy," Rheologica Acta **61**, 355–371 (2022).

[24]P. Cheng, M. C. Burroughs, L. G. Leal, and M. E. Helgeson, "Distinguishing shear banding from shear thinning in flows with a shear stress gradient," Rheologica Acta **56**, 1007–1032 (2017).

[25]J. Yerushalmi, S. Katz, and R. Shinnar, "The stability of steady shear flows of some viscoelastic fluids," Chemical Engineering Science **25**, 1891–1902 (1970).

[26]M. E. Helgeson, M. D. Reichert, Y. T. Hu, and N. J. Wagner, "Relating shear banding, structure, and phase behavior in wormlike micellar solutions," Soft Matter **5**, 3858–3869 (2009).

[27]M. Johnson Jr and D. Segalman, "A model for viscoelastic fluid behavior which allows non-affine deformation," Journal of Non-Newtonian fluid mechanics **2**, 255–270 (1977).

[28]M. Doi, S. F. Edwards, and S. F. Edwards, The theory of polymer dynamics, Vol. 73 (oxford university press, 1988).

[29]M. Cates, "Reptation of living polymers: dynamics of entangled polymers in the presence of reversible chain-scission reactions," Macromolecules **20**, 2289–2296 (1987).

[30]P. A. Vasquez, G. H. McKinley, and L. P. Cook, "A network scission model for wormlike micellar solutions: I. model formulation and viscometric flow predictions," Journal of Non-Newtonian Fluid Mechanics **144**, 122–139 (2007).

[31]H. Giesekus, "A simple constitutive equation for polymer fluids based on the concept of deformation-dependent tensorial mobility," Journal of Non-Newtonian Fluid Mechanics **11**, 69–109 (1982).

[32]A. E. Likhtman and R. S. Graham, "Simple constitutive equation for linear polymer melts derived from molecular theory: Rolie–poly equation," Journal of Non-Newtonian Fluid Mechanics **114**, 1–12 (2003).

[33]G. Ianniruberto and G. Marrucci, "Shear banding in doi–edwards fluids," Journal of Rheology **61**, 93–106 (2017).

[34]A. Briole, L. Casanellas, M.-A. Fardin, C. Py, O. Cardoso, J. Browaeys, and S. Lerouge, "Shear-banding fluid (s) under time-dependent shear flows. part ii: A test of the moorcroft–fielding criteria," Journal of Rheology **65**, 1201–1217 (2021).

[35]P. Rassolov and H. Mohammadigoushki, "Role of micellar entanglements on kinetics of shear banding flow formation," Journal of Rheology **67**, 169–181 (2022).

[36]S. M. Fielding and P. D. Olmsted, "Flow phase diagrams for concentration-coupled shear banding," The European Physical Journal E **11**, 65–83 (2003).

[37]S. M. Fielding and P. D. Olmsted, "Kinetics of the shear banding instability in startup flows," Physical Review E **68**, 036313 (2003).

[38]H. J. Wilson and S. M. Fielding, "Linear instability of planar shear banded flow of both diffusive and non-diffusive johnson–segalman fluids," Journal of Non-Newtonian Fluid Mechanics **138**, 181–196 (2006).

[39]P. D. Olmsted, "Perspectives on shear banding in complex fluids," Rheologica Acta **47**, 283–300 (2008).

[40]P. Olmsted, O. Radulescu, and C.-Y. Lu, "Johnson–segalman model with a diffusion term in cylindrical couette flow," Journal of Rheology **44**, 257–275 (2000).

[41]P. D. Olmsted and C.-Y. Lu, "Coexistence and phase separation in sheared complex fluids," Physical Review E **56**, R55 (1997).

[42]A. Ghadai, P. K. Bera, and S. Majumdar, "Origin of steady state stress fluctuations in a shear-thinning worm-like micellar system," Physics of Fluids **35** (2023).

[43]R. L. Moorcroft and S. M. Fielding, "Criteria for shear banding in time-dependent flows of complex fluids," Physical review letters **110**, 086001 (2013).

[44]S. Sharma, V. Shankar, and Y. M. Joshi, "Onset of transient shear banding in viscoelastic shear start-up flows: Implications from linearized dynamics," Journal of Rheology **65**, 1391–1412 (2021).

[45]S. M. Fielding, "Triggers and signatures of shear banding in steady and time-dependent flows," Journal of Rheology **60**, 821–834 (2016).

[46]J. Cao and A. E. Likhtman, "Shear banding in molecular dynamics of polymer melts," Physical Review Letters **108**, 028302 (2012).

[47]M. Mohagheghi and B. Khomami, "Elucidating the flow-microstructure coupling in entangled polymer melts. part ii: Molecular mechanism of shear banding," Journal of Rheology **60**, 861–872 (2016).

[48]L. Zhou, P. A. Vasquez, L. P. Cook, and G. H. McKinley, "Modeling the inhomogeneous response and formation of shear bands in steady and transient flows of entangled liquids," Journal of rheology **52**, 591–623 (2008).

[49]L. Zhou, L. P. Cook, and G. H. McKinley, "Multiple shear-banding transitions for a model of wormlike micellar solutions," SIAM Journal on Applied Mathematics **72**, 1192–1212 (2012).

[50]L. Zhou, G. H. McKinley, and L. P. Cook, "Wormlike micellar solutions: Iii. vcm model predictions in steady and transient shearing flows," Journal of Non-Newtonian Fluid Mechanics **211**, 70–83 (2014).

[51]M. C. Burroughs, Y. Zhang, A. Shetty, C. M. Bates, M. E. Helgeson, and L. G. Leal, "Flow-concentration coupling determines features of nonhomogeneous flow and shear banding in entangled polymer solutions," Journal of Rheology **67**, 219–239 (2023).

[52]R. Benzi, T. Divoux, C. Barentin, S. Manneville, M. Sbragaglia, and F. Toschi, "Continuum modeling of shear startup in soft glassy materials," Physical Review E **104**, 034612 (2021).

[53]P. Tapadia and S.-Q. Wang, "Direct visualization of continuous simple shear in non-newtonian polymeric fluids," Physical review letters **96**, 016001 (2006).

[54]S. Ravindranath, S.-Q. Wang, M. Olechnowicz, and R. P. Quirk, "Banding in simple steady shear of entangled polymer solutions," Macromolecules **41**, 2663–2670 (2008).

[55]S.-Q. Wang, S. Ravindranath, and P. Boukany, "Homogeneous shear, wall slip, and shear banding of entangled polymeric liquids in simple-shear rheometry: A roadmap of nonlinear rheology," Macromolecules **44**, 183–190 (2011).

[56]P. E. Boukany and S.-Q. Wang, "Use of particle-tracking velocimetry and flow birefringence to study nonlinear flow behavior of entangled wormlike micellar solution: From wall slip, bulk disentanglement to chain scission," Macromolecules **41**, 1455–1464 (2008).

[57]P. E. Boukany and S.-Q. Wang, "Exploring the transition from wall slip to bulk shearing banding in well-entangled dna solutions," Soft Matter **5**, 780–789 (2009).

[58]P. E. Boukany and S.-Q. Wang, "Shear banding or not in entangled dna solutions depending on the level of entanglement," Journal of Rheology **53**, 73–83 (2009).

[59]Y. T. Hu, L. Wilen, A. Philips, and A. Lips, "Is the constitutive relation for entangled polymers monotonic?" Journal of Rheology **51**, 275–295 (2007).

[60]Y. T. Hu, C. Palla, and A. Lips, "Comparison between shear banding and shear thinning in entangled micellar solutions," Journal of Rheology **52**, 379–400 (2008).

[61]Y. Li, M. Hu, G. B. McKenna, C. J. Dimitriou, G. H. McKinley, R. M. Mick, D. C. Venerus, and L. A. Archer, "Flow field visualization of entangled polybutadiene solutions under nonlinear viscoelastic flow conditions," Journal of Rheology **57**, 1411–1428 (2013).

[62]S.-Q. Wang, G. Liu, S. Cheng, P. E. Boukany, Y. Wang, and X. Li, "Letter to the editor: Sufficiently entangled polymers do show shear strain localization at high enough weissenberg numbers," Journal of Rheology **58**, 1059–1069 (2014).

[63]J. D. Peterson, Shear Induced Demixing in Polymer Melts and Solutions, Ph.D. thesis, University of California, Santa Barbara (2018).

[64]S. M. Fielding and P. D. Olmsted, "Early stage kinetics in a unified model of shear-induced demixing and mechanical shear banding instabilities," Physical review letters **90**, 224501 (2003).

[65]M. Cromer, M. C. Villet, G. H. Fredrickson, and L. G. Leal, "Shear banding in polymer solutions," Physics of Fluids **25**, 051703 (2013).

[66]M. Cromer, G. H. Fredrickson, and L. G. Leal, "A study of shear banding in polymer solutions," Physics of Fluids **26**, 063101 (2014).

[67]J. D. Peterson, M. Cromer, G. H. Fredrickson, and L. Gary Leal, "Shear banding predictions for the two-fluid rolie-poly model," Journal of Rheology **60**, 927–951 (2016).

[68]P. Rassolov and H. Mohammadigoushki, "Effects of elasticity and flow ramp up on kinetics of shear banding flow formation in wormlike micellar fluids," Journal of Rheology **64**, 1161–1177 (2020).

[69]P. Rassolov, A. Scigliani, and H. Mohammadigoushki, "Kinetics of shear banding flow formation in linear and branched wormlike micelles," Soft Matter **18**, 6079–6093 (2022).

[70]H. Mohammadigoushki, A. Dalili, L. Zhou, and P. Cook, "Transient evolution of flow profiles in a shear banding wormlike micellar solution: Experimental results and a comparison with the vcm model," Soft matter **15**, 5483–5494 (2019).

[71]M. Alam and P. R. Nott, "The influence of friction on the stability of unbounded granular shear flow," Journal of Fluid Mechanics **343**, 267–301 (1997).

[72]P. J. Schmid and D. S. Henningson, "Optimal energy density growth in hagen–poiseuille flow," Journal of Fluid Mechanics **277**, 197–225 (1994).

[73]P. Schmid and H. Kytömaa, "Transient and asymptotic stability of granular shear flow," Journal of Fluid Mechanics **264**, 255–275 (1994).

[74]G. Strang and K. Borre, Linear algebra, geodesy, and GPS (Siam, 1997).

[75]L. G. Leal, Advanced transport phenomena: fluid mechanics and convective transport processes, Vol. 7 (Cambridge University Press, 2007).

[76]G. C. Georgiou and D. Vlassopoulos, "On the stability of the simple shear flow of a johnson–segalman fluid," Journal of Non-Newtonian Fluid Mechanics **75**, 77–97 (1998).

[77]S. M. Fielding, "Shear banding in soft glassy materials," Reports on Progress in Physics **77**, 102601 (2014).

[78]C.-Y. D. Lu, P. D. Olmsted, and R. Ball, "Effects of nonlocal stress on the determination of shear banding flow," Physical Review Letters **84**, 642 (2000).

[79]R. B. Bird, R. C. Armstrong, and O. Hassager, "Dynamics of polymeric liquids. 2nd ed. : Fluid mechanics," Wiley, New York **1** (1987).

[80]R. Gordon and W. Schowalter, "Anisotropic fluid theory: a different approach to the dumbbell theory of dilute polymer solutions," Transactions of the Society of Rheology **16**, 79–97 (1972).

[81]R. G. Larson, "Chapter 5 – constitutive models with nonaffine motion," in Constitutive Equations for Polymer Melts and Solutions, Butterworths Series in Chemical Engineering, edited by R. G. Larson (Butterworth-Heinemann, 1988) pp. 129–155.

[82]G. A. Holroyd, S. J. Martin, and R. S. Graham, "Analytic solutions of the rolie poly model in time-dependent shear," Journal of Rheology **61**, 859–870 (2017).

[83]P. G. Drazin and W. H. Reid, Hydrodynamic stability (Cambridge university press, 2004).

[84]S. Chandrasekhar, Hydrodynamic and hydromagnetic stability (Courier Corporation, 2013).

[85]E. M. Lifshitz and L. P. Pitaevskii, Statistical physics: theory of the condensed state, Vol. 9 (Elsevier, 2013).

[86]B. Barker, J. B. Bell, and A. L. Garcia, "Fluctuating hydrodynamics and the rayleigh–plateau instability," Proceedings of the National Academy of Sciences **120**, e2306088120 (2023), https://www.pnas.org/doi/pdf/10.1073/pnas.2306088120.

[87]G. Nicolis and I. Prigogine, Self-Organization in Nonequilibrium Systems: From Dissipative Structures to Orde A Wiley-Interscience publication (Wiley, 1977).

[88]J. Adams and P. D. Olmsted, "Nonmonotonic models are not necessary to obtain shear banding phenomena in entangled polymer solutions," Physical review letters **102**, 067801 (2009).

[89]K. Kuperkar, L. Abezgauz, D. Danino, G. Verma, P. Hassan, V. Aswal, D. Varade, and P. Bahadur, "Structural investigation of viscoelastic micellar water/ctab/nano 3 solutions," Pramana **71**, 1003–1008 (2008).